



Numerical Simulation of Tsunami Coastal Amplitudes in the Pacific Coast of Mexico Based on Non-Uniform k^{-2} Slip Distributions

L. VÁZQUEZ,^{1,2} M. MEDINA,³ S. RIQUELME,³ and D. MELGAR⁴

Abstract—Three seismic gaps lie along the Pacific Coast of Mexico, the Tehuantepec, Guerrero, and Colima–Jalisco gaps. In the Tehuantepec seismic gap, there has not been a $M > 7$ earthquake since 1902 until the $M_w = 8.2$ in 2017 which was an intraplate event. Furthermore, there has not been significant seismic activity in the Guerrero gap for over fifty years; therefore, it is considered as potentially likely to produce a major event. Based on historical seismicity and the National Seismological Service of Mexico's earthquakes catalog, the last major earthquake in the Colima–Jalisco gap struck in 1995 with $M_w = 8.0$. To better understand the tsunami hazards due to the generation of near-field tsunamis in Mexico, in this work we characterize hypothetical events of magnitudes $M_w = 8.0$, $M_w = 8.2$, and $M_w = 8.2$ in the Tehuantepec, Guerrero, and Colima–Jalisco gaps, respectively. We generated 99 earthquakes with stochastic k^{-2} finite fault slip distributions and one earthquake with uniform slip distribution at each seismic gap. The non-planar geometry of the megathrust for each rupture area was taken into account. For each seismic gap, we compute the vertical co-seismic displacement by adding up the contribution from all point sources distributed over a grid mesh on each of the faults. Under the passive tsunami generation assumption, we simulated the tsunami wave-field propagation to obtain the coastal amplitude along the Pacific coast of Mexico. The numerical results show likely maximum peak amplitudes of ~ 8 m, ~ 14 m, and ~ 15 m, in Tehuantepec, Guerrero, and Colima–Jalisco gaps, respectively. The uniform slip distribution assumption over stochastic scenarios shows an average underestimation factor of 1.3 for the three seismic gaps. While our computations were carried out carefully and accurately, our models have limitations. Thus, our results cannot be used as an authoritative tsunami hazard assessment.

Keywords: Coastal amplitude, Near-field tsunami, Megathrust earthquake, Earthquake source complexity.

1. Introduction

The Mexican coast has experienced several near-field tsunamis and Fig. 1 shows the seismicity of the last century at the Pacific Coast of Mexico. The largest tsunami in Mexico hit the coast of Oaxaca, on 28 March 1787, generated by a $M8.6$ earthquake (Suárez and Albini, 2009). Some studies suggest that the water reached as far as 6.5 km inland (García and Suárez, 1996; Nuñez-Cornú et al., 2018; Suárez and Albini, 2009; Ramírez-Herrera et al., 2020). It is important to study and understand the consequences of near-field events because the arrival times of the first damaging waves can be short. This is especially true for Mexico where the coast to trench distance can be as short as ~ 30 km. There is little time to order and to evacuate the potentially affected areas. This is in contrast to what we know about far-field tsunamis where the arrival time of the leading wave can be computed in advance, thus providing enough time for the population and authorities to mitigate disaster and human losses (Ruiz et al. 2015).

Several factors control the generation of near-field tsunamis, its propagation and its effects onshore, such as inundation and runup. These include not just the particularities of the source but the complex interactions with the coast and near-shore bathymetry (e.g., Yamazaki and Cheung, 2011; Yamazaki et al., 2011a, b; Lay et al., 2011; Geist, 2002). The destructive tsunamis of the 21st century such as that generated by the 2011, $M_w 9.0$, Tohoku–Oki, Japan, megathrust earthquake, that occurred along the Japanese subduction zone, has spurred much new interest in a better understanding of the tsunami generation process (Ide et al., 2011) and, in

¹ Facultad de Ingeniería, Universidad Nacional Autónoma de México, Mexico City, México. E-mail: luisalbe@usc.edu

² Present Address: Department of Earth Sciences, University of Southern California, Los Angeles, California, USA.

³ Facultad de Ciencias Físicas y Matemáticas, Centro Sismológico Nacional, Universidad de Chile, Blanco Encalada, Santiago 2002, Chile.

⁴ Department of Earth Sciences, University of Oregon, Eugene, Oregon, USA.

particular, its relationship with seismogenic subduction zones (Fujii et al., 2011).

For tsunami modeling propagation and inundation it is important to have good quality input data, such as a high-resolution bathymetry/topography, and a detailed description of the fault geometry, seismic moment, focal mechanism and co-seismic slip distribution (Ruiz et al., 2015). Ruiz et al. (2015) studied the effect of not considering heterogenous slip distributions in order to model a near-field tsunami generated by a hypothetical $M_w = 9.0$ megathrust earthquake in northern Chile, they found that by neglecting the complexity of the source model, the computed runups along the Chilean coast are being underestimated by a factor of ~ 6 . Similarly Melgar et al. (2019) extended this to lower magnitudes and found that indeed the over-simplification of homogenous slip leads to uniformly underestimated tsunami impacts in the near-field. Furthermore, it has been demonstrated that for the vast majority of near-field tsunamis, the rupture kinematics does not affect the source uncertainty and can be neglected (Williamson et al., 2019; Riquelme et al., 2020).

The Pacific Coast of Mexico has been struck by several $M > 7.0$ earthquakes with high potential to generate a tsunami and historical records show 70 tsunamis from 1732 to 2011 (Ramírez-Herrera et al., 2015). The most destructive tsunamis during the last century occurred on 16 November 1925 in Zihuatanejo, Guerrero and 22 June 1932 in Cuyutlán, Colima (Sánchez and Farreras, 1993; Farreras, 1997). 11 m high tsunami waves were recorded from survey measurements at the coasts near the city of Zihuatanejo and Cuyutlán (Sánchez and Farreras, 1993; Farreras, 1997). Although it could be argued that these events released significant strain, recent studies suggest that those tsunamis were not necessarily related to coseismic deformation but rather are due to submarine landslides (Singh et al., 1998; Corona and Ramírez-Herrera, 2012).

Singh et al. (1981) studied the potential locations of seismic gaps and recurrence periods of large, shallow interplate earthquakes along the Mexican subduction zone by combining information from a catalog of nineteenth century's earthquakes, source parameters of large earthquakes, some relocated epicenters of the twentieth century and redetermined

magnitudes of great, shallow earthquakes. They found that Tehuantepec in particular has a lack of large earthquakes in the twentieth and, most likely, in the nineteenth century as well. It is possible that this gap might be aseismic or that it experience large recurrent times. Geodetic studies, while limited in the offshore resolution suggest that there is some fraction of coupling in the gap and that the seismic potential remains high (Franco et al., 2012). Likewise, while there is still debate as to the exact levels of coupling, it is still suggested that both the Guerrero and Colima–Jalisco gaps have a high seismic potential. Colima–Jalisco, meanwhile is thought to have average repeat times between 32 and 56 years (Singh et al., 1981).

With the aim of generating realistic tsunami hazard estimates in the near field of earthquakes in these gaps, the maximum likely earthquake magnitude must be defined. Similarly, we must correctly model the complex heterogenous characteristics of the source that produce the 3D co-seismic vertical displacements of the seafloor that are the initial condition of the resulting tsunami wave-field. As a result of the larger periods of tsunami waves compared to earthquake rupture duration, the passive tsunami generation assumption is plausible, in which, the total rupture time history can be neglected for some events and studies (Ruiz et al., 2015). Furthermore, it has been demonstrated that for the vast majority of near field tsunamis, the rupture kinematics does not affect the source uncertainty and can be neglected when velocities are faster than 1.5 km/s. However, when rupture velocity is slower than 1.5 km/s, the run-up can be amplified and then this is an important parameter to consider (Riquelme et al., 2020). Here we will focus on regular earthquakes, i.e, rupture velocities larger than 1.5 km/s.

Earthquake ruptures are complex processes, and the slip of past earthquakes imaged through waveform inversion shows spatial heterogeneities at various scales and a dependence on the earthquake sizes (e.g., Mai and Beroza, 2002). Even for the same event, the co-seismic slip of the 2011, $M_w = 9.0$, Tohoku–Oki earthquake, imaged using different inverse methodologies and dataset presents also strong spatial variability, where the peak-slip amplitude obtained ranges from 40 to 80 m (e.g., Simons

et al., 2011; Yagi and Fukahata, 2011; Lay et al., 2011; Yoshida et al., 2011). As a consequence, defining a single uniform slip distribution over an extended source area is an over-simplification of a more complex, but realistic, process. The need of a complete description of heterogeneous slip distributions in order to characterize earthquake source complexity must be done in order to achieve a more physical representation of the seismic source (Ruiz et al., 2015).

The aim of this work is to model near-field tsunamis in three different locations along the Pacific Coast of Mexico, specifically in Oaxaca–Chiapas, Guerrero, and Colima–Jalisco states of Mexico by presenting a case study in each region and, thus modeling the tsunami in the near-field. The target zones are the Tehuantepec (TGap), Guerrero (GGap), and Colima–Jalisco (JGap) seismic gaps. We generate 99 stochastic k^{-2} slip distributions and one uniform slip distribution over a non-planar fault geometry in each of the seismic gaps. After these distributions have been generated, the vertical coseismic displacements are computed. The passive tsunami generation approach is used for every slip distribution, and the coastal amplitudes along the Pacific Coast of Mexico are obtained. The goal of this paper is of pure scientific interest and our results cannot be interpreted as tsunami hazard assessment.

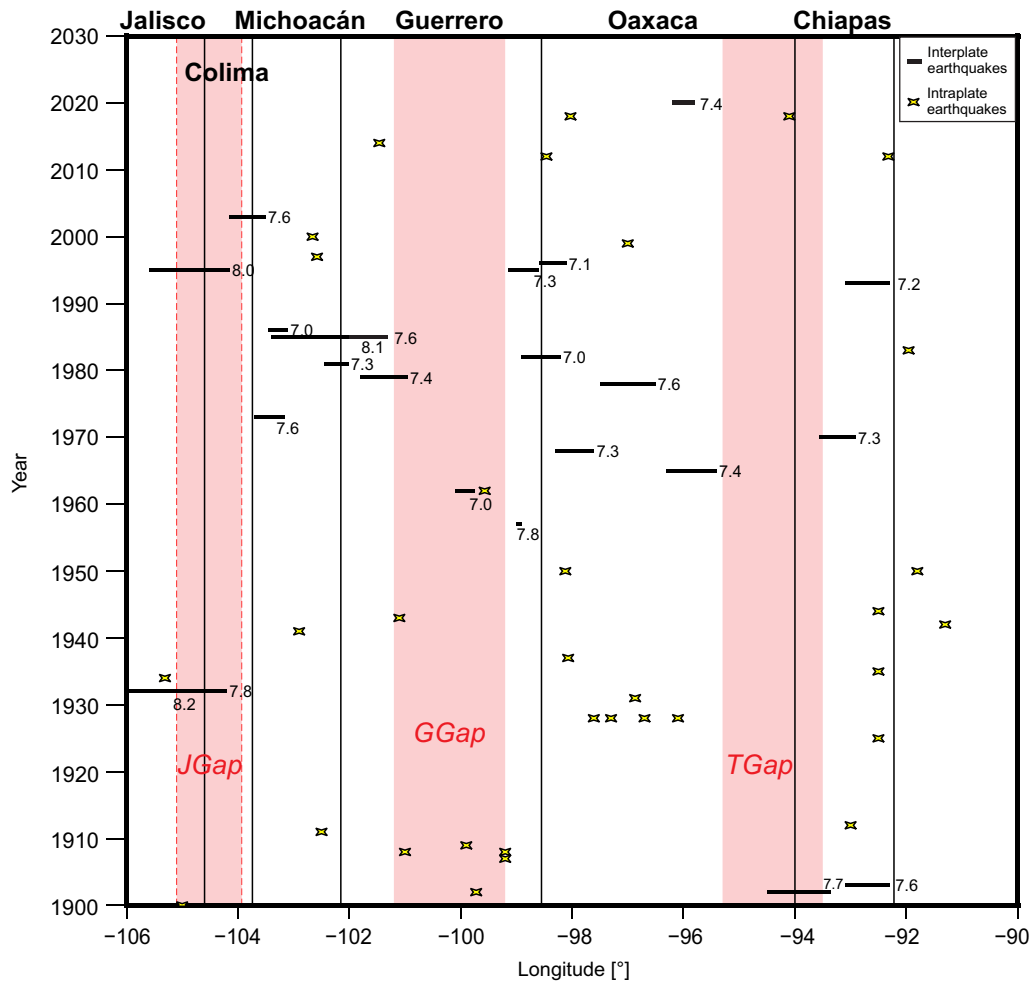
2. Earthquake Rupture for Three Hypothetic Scenarios in the Pacific Coast of Mexico

2.1. Historical Large Earthquakes in the Tehuantepec, Guerrero, and Colima–Jalisco Seismic Gaps

The central-southern Pacific Coast of Mexico is a convergent margin, related to the subduction of Cocos plate underneath the North American and Caribbean plates, with convergence rates of nearly 6.5 cm/year (e.g., Gripp and Gordon, 2002). Our first study area, the Tehuantepec gap (TGap), covers from Salina Cruz to Pijijiapan in the states of Oaxaca and Chiapas, respectively (between the longitudes 93.5° W and 95.3° W) (Fig. 1). The second region of interest, the Guerrero gap (GGap), covers from the

towns of Coyuquila to Copala in the state of Guerrero (between the longitudes 99.2° W to 101.2° W) (Fig. 1). The third and last study area, the Colima–Jalisco gap (JGap), extends from the southernmost portion of Jalisco to the border between Colima and Michoacan states (between the longitudes 103.9° W and 105.1° W) (Fig. 1), i.e., we model a M_w 8.2 in the M_w 8.0 1995 Colima earthquake rupture area. TGap has perhaps the most worrying lack of $M_w \geq 7.0$ interplate earthquakes in the last century with only one $M7.7$ earthquake in 1902 (Singh et al., 1981; SSN's catalog). Thus, we suggest a large but plausible M_w 8.0 megathrust earthquake in this gap. In the last one hundred years, the GGap has experienced only one $M7.0$ event with a depth less than 15 km. The most recent $M_w \geq 7.0$ earthquake that struck the gap, the 18 km deep Petatlan earthquake, is a reminder of what we could expect. This earthquake occurred in 2014 initiating outside the gap and halting right at the western edge of the gap (Cruz-Atienza et al., 2018). Based on these previous works, we consider an event with M_w 8.2 as likely to happen in the near future. In the twentieth century, the JGap has experienced a lack of interplate events, in 1932 a M_w 8.2 struck the region, rupturing from approximately 105° W– 106° W (Singh et al., 1981), after this megathrust earthquake, in 1995, a M_w 8.0 ruptured part of the gap, with longitudes ranging from 104.15° W to 105.60° W (Ortiz et al., 2000). Even though the 1995 event might seem to have ruptured a wider area than the 1932 earthquake, its length in latitude is smaller (Kostoglodov and Pacheco, 1999). Based on these facts, a M_w 8.2 event, while large in magnitude, is plausible (Blaser et al., 2010). The three hypothetical earthquake magnitudes were proposed considering the scaling relationships discussed in Blaser et al. (2010) and on historical seismicity.

Tsunamis that took place after 1952 in Mexico have been recorded by tide gauge stations and from post-tsunami measurements or visual observations (Ramírez-Herrera et al., 2015). Farreras (1997) and Sánchez and Farreras (1993) reported 34 tsunamis generated by earthquakes in the Mexican Subduction Zone. The maximum height recorded at tide-gauge stations is 3 m. Nevertheless, historical data for the last 300 years suggest that the maximum heights



◀Figure 1

Historical seismicity. Top, map of Mexico. Bottom, historic events with their year of occurrence and its location along the subduction zone, the red dashed vertical lines represent the edges of each gap, while the black solid vertical lines are the boundaries of the states of Mexico named in the text. The yellow stars are the intraplate earthquakes that occurred in the last century and the black solid horizontal lines are the rupture area along the longitude of interplate earthquakes (Singh et al., 1981, SSN's catalog)

along the Pacific coast of Mexico can be much larger than those reported in the last 60 years from tide-gauge observations.

The Mexican historical tsunami database has a lack of records due to a small number of carried out post-tsunami field surveys. Post-tsunami field data were reported only after the 19 and 20 September 1985 Michoacán earthquakes (Abe et al., 1986) and the 9 October 1995 Colima–Jalisco M_w 8.0 earthquake (Borero et al., 1997; Ortiz et al., 1998). More recently, Ramírez-Herrera et al. (2018) conducted a post-event survey following the 8 September 2017 M_w 8.2 Tehuantepec normal faulting event.

Despite of the lack of tsunami database in Mexico, historical tsunami activity in Guerrero has been relatively well-documented. There have been a total of 31 tsunamis reported along the coast of this state between 1537 and 2012 (Table 1). The information is sparse in most of the cases since the population density has been historically low in the Pacific Coast of Mexico. Only the events listed as numbers 18, 27, and 28 on Table 1 were reported as affecting Zihuatanejo and Ixtapa, the other events have been reported only for Acapulco, which is the oldest and most populated locality along the coast of Guerrero since colonial times (Table 1). We do not report tables as detailed as (Table 1) for other regions due to the lack of past tsunami records in Mexico. However, a recent study by Santos-Reyes (2020) gathered tsunami wave heights for other regions in the Pacific Coast of Mexico (Table 2). Colima have records of tsunami wave amplitudes of up to 5.1 m, these amplitudes were generated by the 1995 M_w 8.0 Colima–Jalisco earthquake. Historical tsunami wave heights have been reported in Jalisco, ranging from 1 to up to 10 m. On the other hand, we only report one

Table 1
Data of 31 earthquakes in Guerrero, Mexico

Historical tsunami recorded in Acapulco, Guerrero state

Event	Date	Maximum water height (m)	Seismic magnitude (Ms)	Event	Date	Maximum water height (m)	Seismic magnitude (Ms)
1	1537	^a	^a	18	1925-11-16	11 ^b	7
2	1732-02-25	3	^a	19	1950-12-14	0.3	7.5
3	1754-09-01	4	^a	20	1957-07-28	1.3	7.9
4	1784-03-28	3	^a	21	1962-05-11	0.81	7
5	1787-03-28	4	8.6	22	1962-05-19	0.34	7.2
6	1820-05-04	4	7.6	23	1965-08-23	0.4	7.8
7	1833-03-10	^a	^a	24	1973-01-30	0.43	7.5
8	1834-03-14	^a	7	25	1979-03-14	1.3	7.6
9	1845-04-07	^a	8	26	1981-10-25	0.9	7.3
10	1852-12-04	^a	7	27	1985-09-19	1.15	8.1
11	1854-12-04	^a	^a	—	—	1.5 ^c	—
12	1860-03-17	^a	^a	—	—	3 ^b	—
13	1868-05-25	^a	^a	28	1985-09-21	1.2	7.6
14	1868-08-12	^a	^a	—	—	1.2 ^b	—
15	1903-07-16	^a	^a	29	1995-09-14	^a	7.2
16	1907-04-14	2	8.3	30	2003-01-22	0.35	7.6
17	1909-07-30	9 ^d	7.8	31	2012-03-20	0.2	7.6

We present the date of occurrence, the maximum tsunami wave amplitude generated by such seismic event, and its seismic magnitude. The symbol ^a stands for undefined measurements, ^b recorded in Zihuatanejo, ^c recorded in Ixtapa, and ^d is interpreted as horizontal inundation. Modified from Ramírez-Herrera et al. (2015)

Table 2

Data of 7 earthquakes at different locations at Pacific Coast of Mexico

Historical tsunami records at the Pacific Coast of Mexico			
Place	Date	Maximum water height (m)	Seismic magnitude
Jalisco	1932-06-03	3	8.2
Jalisco	1932-06-18	1	7.8
Jalisco	1932-06-22	10 ^a	6.9
Oaxaca	1978-11-29	1.5	7.6
Colima	1995-10-09	5.1 ^b	8.0
Colima	2003-01-21	1.22	7.8
Chiapas	2017-09-08	1.1	8.2

We present the place, date of occurrence, maximum tsunami wave amplitude generated by such seismic event, and its seismic magnitude. The Measurement ^a is speculated to be the result of a submarine slump, ^b maximum reported value. Modified from Santos-Reyes (2020)

mearurement for TGap, a 1.1 m high tsunami generated by the 2017 M_w 8.2 Chiapas earthquake.

2.2. Setting Non-Planar Complex Rupture Fault Geometries

We assumed three fault zones extending from Salina Cruz to Pijijiapan, from Coyuquilla to Copala, and finally from the sourthernmost portion of Jalisco to the border between Colima and Michoacan, corresponding to the seismic gaps of Tehuantepec, Guerrero, and Colima–Jalisco, respectively. Because the seismogenic plate interfaces are complex, we construct non-planar geometries for each gap in order to represent the earthquake slip surface.

In the TGap, to define the non-planar fault, we use 94°W and 14.15°N as the southwest vertex of the fault. The top of fault is buried at 8.5 km at the trench axis, meaning that the rupture does not reach the free surface, thus, a buried rupture is assumed. We define only one segment along strike going northward with length and strike of 160 km and 304°, respectively. The rupture surface was defined with two downdip consecutive segments, the shallower segment (blue segment in Fig. 2) is set to have a width of 20 km and a dip of 8°, and the deeper segment (red segment in Fig. 2) is 60 km wide with a dip of 14°. The approximate downdip geometry was determined from USGS Slab 2.0 model (Hayes, 2018) between the longitudes 99.2°W and 101.2°W. The total fault width is 80 km, and the deepest fault zone also reaches approximately 25 km. An example of the constructed mesh composed by planar quadrilateral elements is shown in (Fig. 3).

longitudes 93.5°W and 95.3°W. The total fault width is 80 km, and the deepest fault zone reaches approximately 25 km. We define local coordinates along the strike and dip and, therefore, we can define N_x and N_y subfaults along strike and dip, respectively, in order to mesh the fault surface. An example of the constructed mesh composed by planar quadrilateral elements is shown in (Fig. 2).

The total fault area is about 12800 km². The non-planar complex fault geometry is compared against the Slab 2.0 model (Hayes, 2018) at three cross sections (Fig. 2, right). No differences are observed at neither of the profiles along the fault.

The lower boundary of the seismically coupled interface is located at approximately 25 km, as discussed by Pardo and Suárez (1995).

In GGap, we located the coordinate origin at 99.20°W and 16.20°N. The top fault is buried at 8.5 km at the trench axis. We define only one segment along strike going northward with length and strike of 220 km and 293.8°W, respectively. The rupture surface was defined with two downdip consecutive segments. The red segment in Fig. 3) shows the shallower subfault to have a width of 20 km and a dip of 8°, and the deeper segment is 60 km wide with a dip of 14°, red segment in Fig. 3. The approximate downdip geometry was determined from USGS Slab 2.0 model (Hayes, 2018) between the longitudes 99.2°W and 101.2°W. The total fault width is 80 km, and the deepest fault zone also reaches approximately 25 km. An example of the constructed mesh composed by planar quadrilateral elements is shown in (Fig. 3).

The total fault area is about 17600 km². The non-planar complex fault geometry is compared against the Slab 2.0 model (Hayes, 2018) at three cross sections (Fig. 3, right). No differences are observed at neither of the profiles along the fault.

The lower boundary of the seismically coupled interface is located at approximately 25 km, as discussed by Pardo and Suárez (1995).

Lastly, in JGap, we located the coordinate origin at 103.90°W and 18.18°N. The top fault is buried at 6.2 km at the trench axis. We define only one segment along strike going northward with length and strike of 150 km and 295°, respectively. The rupture surface downdip was defined with three segments, the

shallower segment (green segment in Fig. 4) is set to have a width of 20 km and a dip of 10° , the middle segment (blue segment in Fig. 4) is 40 km wide with a dip of 26° , and the deeper segment (red segment in Fig. 4) is 30 km wide with a dip of 34° . The approximate downdip geometry was determined from USGS Slab 2.0 model (Hayes 2018) between the longitudes 103.9°W and 105.1°W . The total fault width is 90 km, and the deepest fault zone reaches approximately 25 km. An example of the constructed mesh composed by planar quadrilateral elements is shown in (Fig. 4)

The total fault area is about 13500 km^2 . The non-planar complex fault geometry is compared against the Slab 2.0 model (Hayes, 2018) at three cross sections (Fig. 4, right). Minor differences are observed at the north and south profiles; however, we consider they are the closest approximation of the real slab geometry.

The lower boundary of the seismically coupled interface is located at approximately 40 km, as discussed by Pardo and Suárez (1995).

2.3. Stochastic Complex Earthquake Rupture Model

The method to generate heterogenous sources are based on the Ruiz et al. (2015) paper. We focused our analysis on the spatial variability of the source and neglected the kinematic effects, thus very slow earthquakes are not modeled in this study.

Some studies (e.g., Geist and Dmowska, 1999; Geist, 2002) have shown that the spatially heterogeneous co-seismic slip controls the tsunami wave amplitudes. Geist and Dmowska (1999) showed that nonuniform slip, particularly in the dip direction for subduction zone events, has an important effect on the static vertical displacement field and therefore, in the tsunami generation as well. Geist (2002) suggested that variability in local tsunamis run-up scaling can be ascribed to tsunami source parameters that are independent of seismic moment: variations in the water depth in the source region, the combination of higher slip and lower shear modulus at shallow depths, and rupture complexity derived from spatially heterogeneous slip distributions. Inspired by these works, we generated spatially heterogeneous slip

distributions using the stochastic k^{-2} earthquake source model for near-field tsunami modeling.

Andrews (1980) showed that if the slip spectrum amplitudes falloff as k^{-2} in the wavenumber domain, then the source radiates a far-field displacement spectrum that obeys the ω^{-2} model proposed by Aki (1967). Herrero and Bernard (1994), based on the ideas proposed by Andrews (1980), introduced the k^{-2} self-similar source model making the slip spectrum decay as k^{-2} beyond a corner wavenumber, k_c , defined as $k_c = 2\pi/L_c$. L_c is usually related to fault width or length.

To obtain a slip distribution, a 2D stochastic spatial random field needs to be computed to later impose the k^{-2} spectral decay of the 2D Fourier amplitude of the slip at high wave numbers (e.g., Andrews, 1980; Herrero and Bernard, 1994).

The 2D Fourier slip spectrum can be expressed as being proportional to,

$$\Delta\tilde{u}(k) \propto \frac{1}{1 + (\frac{k}{k_c})^2} e^{i\phi(k)} \quad (1)$$

where $\phi(k)$ is the spectral phase, $k = \sqrt{k_x^2 + k_y^2}$ is the radial number, and k_x and k_y are the wavenumber components in the x and y directions, respectively. To randomly generate the spatially heterogeneous slip distributions, random phases are introduced to (Eq. 1) when $k > k_c$, while at shorter wavenumbers, a coherent phase distribution is imposed. As previously shown, the k^{-2} spectral decay is imposed in the wavenumber domain, after this spectral behavior is assured, the inverse 2D FFT is applied in order to have the slip distributions in the spatial domain $\Delta u(x, y)$. In order to avoid high stress concentrations, the slip is tapered to avoid nonzero slip amplitude at the edges of the fault. We use the correlation lengths from Mai and Beroza (2002). Finally, the tapered slip is normalized to the target seismic moment.

Figure 5 shows a numerical realization of a stochastic k^{-2} slip distribution for a $M_w 8.2$ earthquake in the Guerrero gap. As discussed in the Subsect. 2.2, for GGap, $A_{total} = 17600\text{ km}^2$, and the width of the fault is 80 km, therefore, $L_{avg} = A_{total}/W$, and this gives $L_{avg} = 220\text{ km}$, where A_{total} is the total fault surface. The fault was subdivided in a regular grid mesh of $N_x \times N_y = 110 \times 40$ subfaults. The slip distribution is

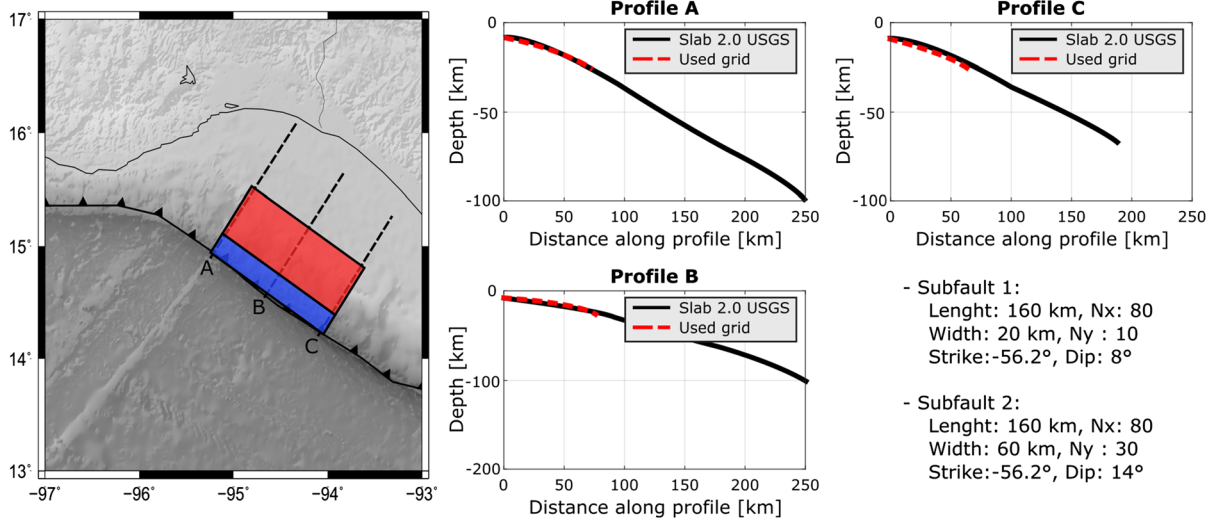


Figure 2

Rupture fault geometry for TGap. 15 arc-s bathymetry in Tehuantepec Gap and non-planar mesh that defines the rupture for a $M_w 8.0$ megathrust earthquake breaking the TGap are shown at the left. Three cross sections orthogonal to the trench axis are shown at the right. In each profile, the downdip fault geometry (red dashed line) is compared against the USGS Slab 2.0 (black solid line) (Hayes, 2018)

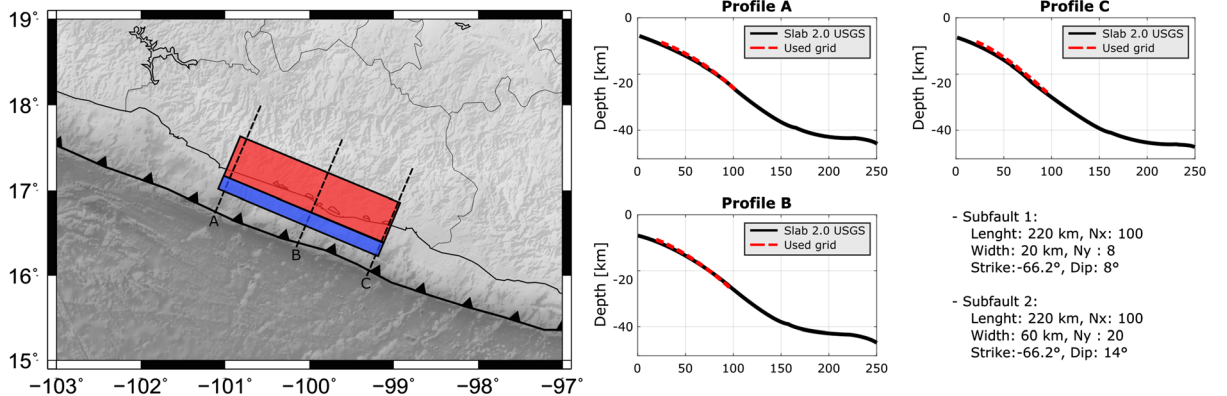


Figure 3

Rupture fault geometry for GGap. 15 arc-s bathymetry in Guerrero Gap and non-planar mesh that defines the rupture for a $M_w 8.2$ megathrust earthquake breaking the GGap are shown at the left. Three cross sections orthogonal to the trench axis are shown at the right. In each profile, the downdip fault geometry (red dashed line) is compared against the USGS Slab 2.0 (black solid line) (Hayes, 2018)

heterogeneous both along the dip and along the strike (Fig. 5, left), and the 2D Fourier amplitudes of the slip decay as k^{-2} (Fig. 5, right).

2.4. Modeling Co-Seismic Static Displacement Field for Complex Slip Earthquake

We follow the Okada's (1992) formulas that compute internal static displacements and strain due

to shear and tensile faults buried in a homogeneous elastic halfspace for point source and finite rectangular faults. The 3D static displacement field at the free surface is computed by assuming a discrete point-source approach for an extended seismic source.

The static vertical displacement field for one uniform and 99 stochastic scenarios was computed.

We only show one example for each proposed seismic gap in this study.

Figure 6 shows the TGAP results of one numerical realization for the heterogeneous k^{-2} and uniform slip distributions, and their respective displacement fields in (Fig. 8). In this particular case, the maximum slip reached a value of approximately 8 m, which is located in two patches at both deep and shallow zones of the finite fault. The corresponding co-seismic static vertical displacement field shows its maximum values of approximately 2 m at high slip zones. The uplift is located seaward, while the subsidence is located landward. The uniform simulation shows a slip and a deformation value of 3 m and 1 m, respectively.

Figure 7 shows the results of one numerical realization for the heterogeneous k^{-2} and uniform slip distributions, and their respective displacement fields in the Guerrero gap. In this particular case, the maximum slip reached a value of approximately 14 m, which is located at the deepest zone of the rupture area. The corresponding co-seismic static vertical displacement field shows its maximum values of 2–3 m at high slip zones. The uplift is located seaward, while the subsidence is located landward. Furthermore, the uniform slip shows a value of 4 m and a maximum deformation of approximately 1 m.

Finally, Fig. 8 shows the results of one numerical realization for the heterogeneous k^{-2} and uniform slip distributions, and their respective displacement fields in the Colima-Jalisco gap. In this particular case, generated by a heterogeneous slip distribution, the maximum slip reached a value of approximately 20 m, which is located updip near the trench. The corresponding co-seismic static vertical displacement field shows its maximum values of 3.5 m at high slip zones. The uplift is located seaward, while the subsidence is located landward. The uniform slip shows a value of 5 m and a deformation of 3 m.

3. Near-Field Tsunami Coastal Amplitudes Modeling

In the next two sections, we present the results from numerical simulations of near-field tsunamis for one uniform and 99 heterogeneous k^{-2} slip distributions of three cases of study assuming $M_w 8.2$, $M_w 8.2$,

and $M_w 8.0$ earthquakes in Jalisco-Colima, Guerrero, and Tehuantepec seismic gaps, respectively.

3.1. Initial Condition for Tsunami Modeling

We compute the numerical simulations under the passive generation of tsunamis, neglecting the dynamic seabed displacement generated by the rupture process. The initial condition for tsunami propagation is obtained directly from translating the final static vertical displacement field to the water free surface, thus, we compute the hydrodynamics in space and time. The passive generation of tsunamis is acceptable because the total rupture time for a regular tsunamigenic earthquake is shorter than the period of the propagating water waves.

3.1.1 Tsunami Numerical Model

We use a tsunami numerical model, NEOWAVE (Non-hydrostatic Evolution of Ocean WAVES), that solves the depth-integrated nonlinear shallow water wave equations that account for a non-hydrostatic pressure through a vertical velocity term to describe weakly dispersive waves and a momentum conservation scheme to handle flow discontinuities, such as bores or hydraulic jumps, based on a staggered finite difference technique (Yamazaki et al., 2009, 2011a). A wet/dry moving boundary is implemented for detail inundation/run-up modeling along the coast and full wave transmission at the open sea. It has been previously shown that NEOWAVE is a powerful tool to study near-field tsunami from its generation, propagation and inundation processes (e.g., Yamazaki et al., 2011a, b; Lay et al., 2013), and it has been also applied to understand shelf resonance effects of near-field tsunami (Yamazaki and Cheung, 2011). Additionally, this tsunami numerical model has been validated and verified for tsunami propagation and inundation using the analytical, laboratory, and field benchmark tests described by Synolakis et al. (2008).

3.1.2 Model Setup

Due to the different geographic locations of the three proposed seismic gaps, we defined three computational domains. For TGAP (Fig. 9a), the

computational domain ranges from 14° N to 22° N and from 99° W to 91° W. For GGap (Fig. 10a), the computational domain ranges from 14° N to 22° N and from 106° W to 94° W. Finally, for JGap (Fig. 11a), the computational domain ranges from 14° N to 22° N and from 110° W to 100° W. The simulations run for the elapsed time of 6 h using a time step $\Delta t = 1$ s. We set a global grid with a spacing resolution of 15 arc-s (450 m). The Manning coefficient is set up as 0.025, and the vertical wall condition is used at the shore; meaning that the coastal inundations are computed with this boundary condition at the coastline. The bathymetry used is the one available online through the GEBCO (General Bathymetric Chart of the Oceans) (Smith and Sandwell, 1997; Becker et al., 2009).

It has been observed that for portions of the southern Mexican coast the GEBCO data can have inaccuracies, especially for the near source region. There can be some small spurious coastal features. There are higher quality datasets provided by the Mexican navy from gridded multi-beam sonar data. However these have very reduced footprints and only exist for selected ports and coastal towns of importance. In light of this, open datasets like GEBCO remain the best choice for regional modeling. Using datasets like this Gusman et al. (2017) and Melgar

et al. (2018) were able to recreate the tide gauge recordings of the post-event tsunami survey for the 2017 M8.2 Tehuantepec earthquake. Similarly, Melgar et al. (2021) were able to recreate the basic features of tide gauge recordings during the M7.4 La Crucecita earthquake in Oaxaca. In light of this, and because we are not performing inundation modeling and are simply interested in the tsunami amplitudes at the ocean/land boundary, the inaccuracies in GEBCO are a minor concern.

3.1.3 Setting Scenarios for a Set of Stochastic k^{-2} slip

We computed 99 heterogeneous k^{-2} slip distributions for three hypothetical M_w 8.0, M_w 8.2, and M_w 8.2 megathrust earthquakes in Tehuantepec, Guerrero, and Jalisco–Colima seismic gaps, respectively. Based on Ruiz et al. (2015), this number of computations represents a good compromise in terms of computational time and storage, to generate reliable results in terms of tsunami modeling. For each slip, we computed the co-seismic vertical displacement field. The finite fault geometry follows the complex non-planar geometry of the seismogenic plate interface proposed in this study. For the whole set of slips, the target magnitudes, M_w 8.0, M_w 8.2, and M_w 8.2, and the total respective rupture areas are fixed. For each slip

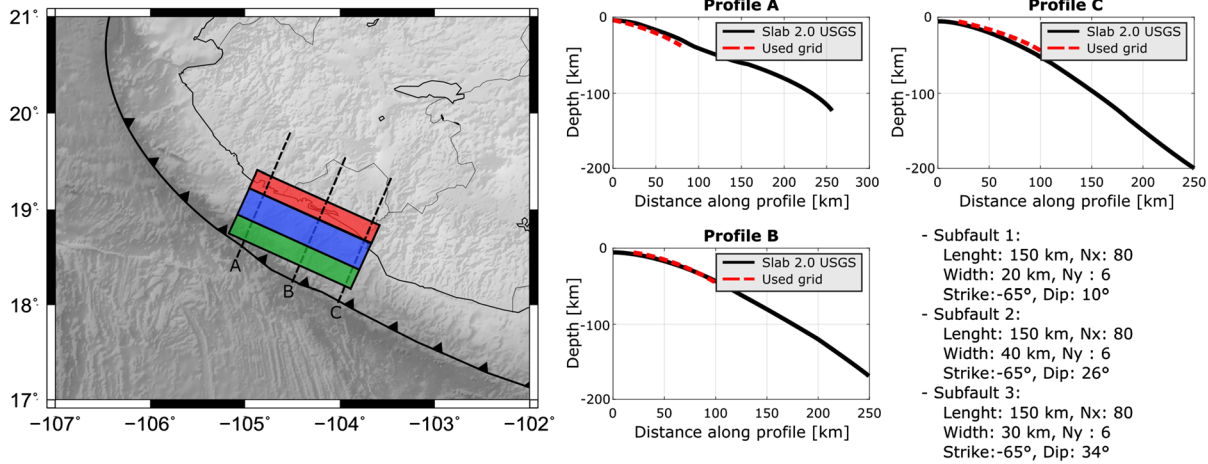


Figure 4

Rupture fault geometry for JGap. 15 arc-s bathymetry in Jalisco–Colima Gap and non-planar mesh that defines the rupture for a M_w 8.2 megathrust earthquake breaking the JGap are shown at the left. Three cross sections orthogonal to the trench axis are shown at the right. In each profile, the downdip fault geometry (red dashed line) is compared against the USGS Slab 2.0 (black solid line) (Hayes, 2018)

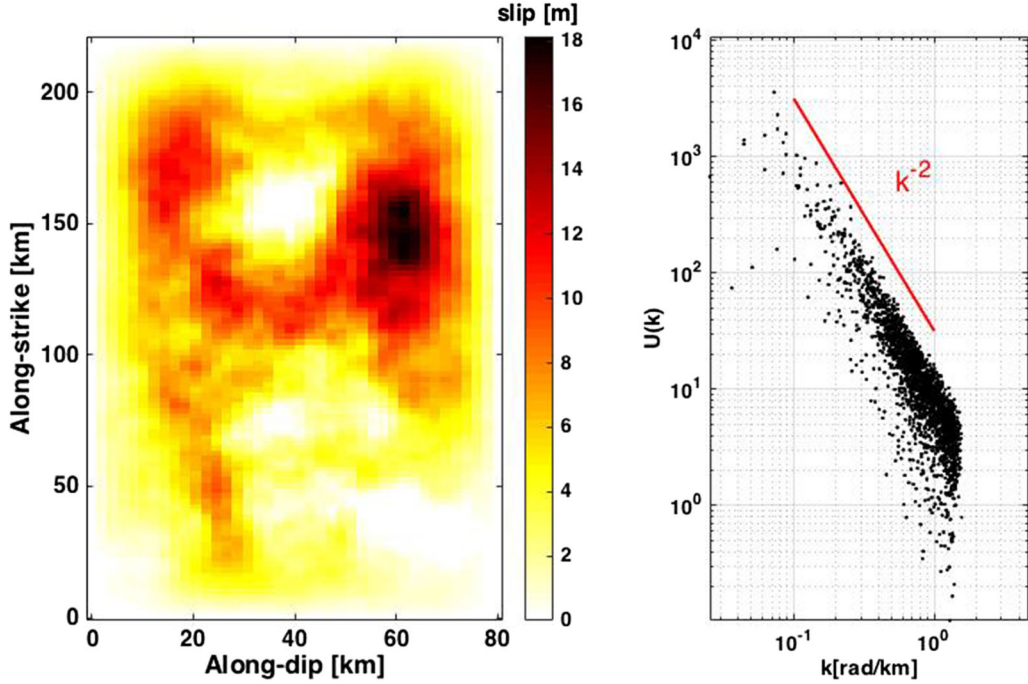


Figure 5

Numerical realization of a stochastic k^{-2} slip distribution for a $M_w 8.2$ earthquake in the Guerrero gap. We show the spatial distribution, and amplitude of the 2D Fourier spectrum of the slip as function of the radial wavenumber k on the left and on the right, respectively

distribution, we model the tsunami propagation using NEOWAVE and we also calculate the coastal amplitudes distribution along the coastline.

3.2. Analysis of the Results

Fig. 9 shows the complete set of coastal amplitudes as a function of longitude for Tehuantepec seismic gap located in the region shown in Fig. 9a. Figure 9b shows that the maximum values are > 7 m between 93.3° W and 93.7° W, as well as at 94.6° W. The minimum amplitude value varies between 0 to up to 2.5 m. Moreover, the uniform slips generate a maximum coastal amplitude of approximately 3 m at 93.5° W. The uniform results generally emulate the minimum stochastic behavior; however, this behavior has an exception in the range from 95° W to 96° W where the uniform amplitudes are considerably larger than the minimum stochastic values.

The results for Guerrero seismic gap are plotted in Fig. 10 as function of longitude. Figure 10b shows the complete set of coastal amplitudes for this seismic

gap. The maximum value for this region reached 14 m located at 100.6° W and at 99.8° W as well. The minimum bound fluctuates between 0 and 3 m. The uniform coastal amplitude is generally larger than the minimum stochastic simulation but smaller than most of the other non-uniform simulations. The maximum uniform values are approximately 6 m. We can make further comparison of our GGap results with historical records summarized in Table 1. The mean coastal amplitude for this gap lies within the 3–5 m interval. A $M_s 8.6$ in 1787 produced water heights of up to 4 m in Acapulco, another $M_s 7.6$ in 1820 generated heights of 4 m as well, and a $M_w 7.8$ in 1909 has historical records of 9 m in Acapulco. A more recent $M_s 7.0$ earthquake excited water heights of up to 11 in Zihuatanejo which is somewhat consistent with the maximum coastal amplitude of 9 m for this gap.

The complete set of coastal amplitudes for our numerical simulations in Jalisco–Colima seismic gap is shown in Fig. 11 as a function of longitude. Maximum, minimum and the other 97 amplitude

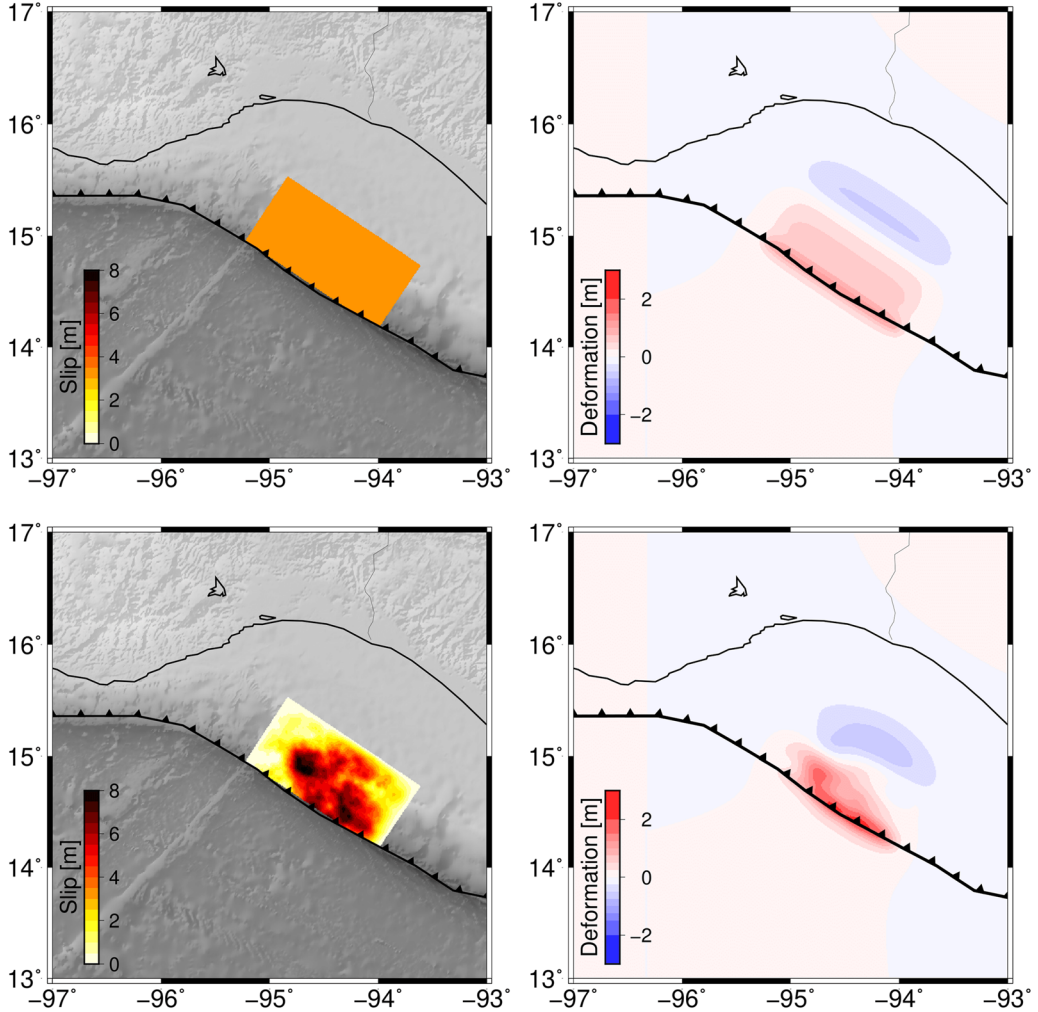


Figure 6

Example of the vertical static displacement modeled for a $M_w 8.0$ megathrust earthquake in Tehuantepec gap when assuming a heterogeneous k^{-2} slip distribution (lower subplot) and an uniform slip distribution (upper subplot) over a non-planar geometry. On the left, we observe their slip distributions. On the right, we show the resulting vertical displacement fields

values as well as the uniform distribution results for JGap are shown in Fig. 11b. The maximum coastal amplitude is approximately 15 m located at nearly 104.5° W, the minimum value is 0 m located westward of 106.7° W. The uniform coastal amplitude shows a pattern that mimics the minimum stochastic amplitude with a few exceptions for which the latter is slightly bigger than the former. The maximum uniform amplitude is 7 m.

Tsunami wavefields generated by the hypothetical earthquakes are shown in Fig. 12. These scenarios were randomly chosen out of the stochastic pool;

however, neither of these represent the maximum nor the minimum, we present scenario number 45 at each seismic gap. We show the tsunami wavefield for the Tehuantepec seismic gap in Fig. 12a, where we observe ocean wave heights of up to 2.5 m not only above the earthquake rupture area, but also along the source-continent path, as well as along the coastline. The scenario for Guerrero seismic gap shows maximum wave heights of up to 2.5 m that are reached above the rupture area as well as along the shore (Fig. 12b). Finally, the results that were obtained for the Jalisco-Colima seismic gap (Fig. 12c) show wave

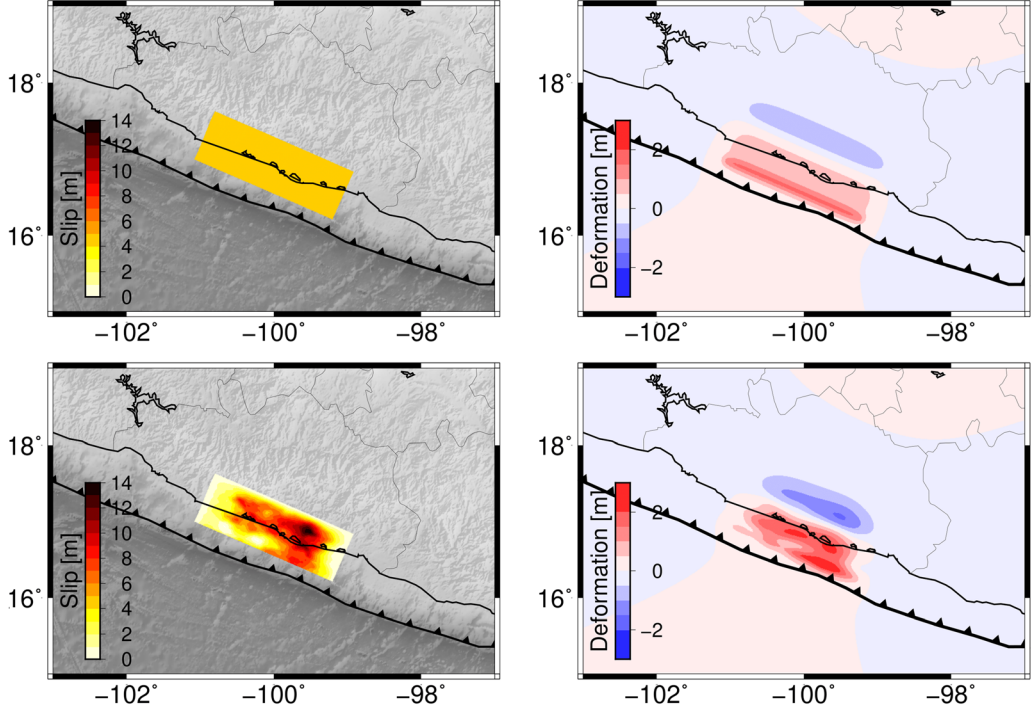


Figure 7

Example of the vertical static displacement modeled for a $M_w 8.2$ megathrust earthquake in Guerrero gap when assuming a heterogeneous k^{-2} slip distribution (lower subplot) and an uniform slip distribution (upper subplot) over a non-planar geometry. On the left, we observe their slip distributions. On the right, we show the resulting vertical displacement fields

amplitudes of approximately 5 m localized at the earthquake rupture area and along the shore. These scenarios are produced by the slip stochastic slip distributions shown in Figs. 6, 7, 8. Figure 12a shows the tsunami wavefield and wave amplifications can be observed along the coast as well as throughout the source-continent path. Similar wave amplifications for the $M_w 8.2$ Tehuantepec earthquake in 2017 are discussed by Melgar et al. (2018) and are suggested to be a result of wholesale resonance of the shelf as well as efficient trapping of edge waves at the shore. The 2017 Tehuantepec earthquake generated a tsunami that lasted as long as three days.

We furthermore computed the statistics for the 99 stochastic scenarios at different longitudes along the coastline (Fig. 13). Our null hypothesis is defined such that the coastal amplitudes follow a log normal distribution. We use the Chi-squared test to statistically compute the probability that the amplitude distributions follow the log normal density function,

e.g., large values represent considerable differences and small values suggest a good agreement. As an additional statistic, we obtain the p values at a 95% of confidence, if we obtain p values smaller than 0.05, we then reject our null hypothesis. We finally compute the coefficient of variation to measure the spread of our data around the mean for the coastal amplitude distributions and the log normal fits. Fig. 13a demonstrates that the TGap amplitudes show a good agreement with a log normal distribution, i.e., the Chi-squared statistics at the seven locations shown in fig. 13a are small and the p values are larger than 0.05. Moreover, the GGap the empirical distributions follow the log normal distribution with the exception at a latitude of 104.41° W where the p value is smaller than 0.05 (Fig. 13b). Finally, according to Fig. 13c, the JGap amplitudes do not follow the proposed log normal distribution only at 99.69° W.

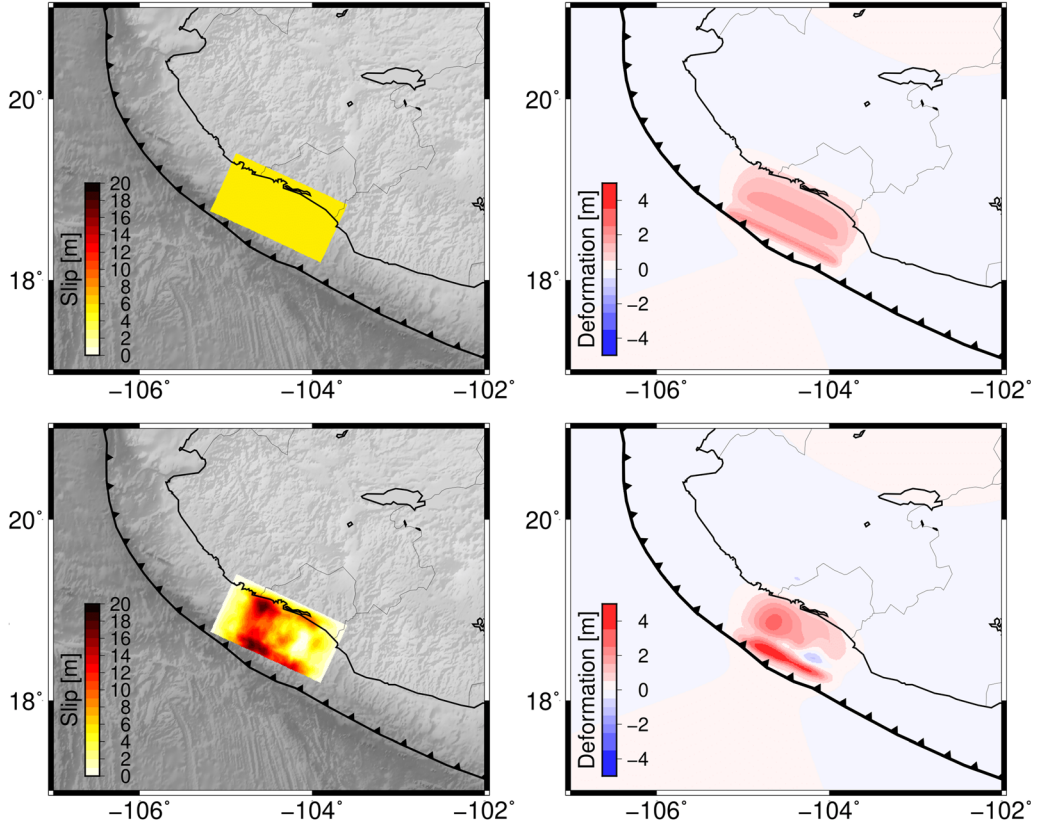


Figure 8

Example of the vertical static displacement modeled for a $M_w 8.2$ megathrust earthquake in Colima-Jalisco gap when assuming a heterogeneous k^{-2} slip distribution (lower subplot) and an uniform slip distribution (upper subplot) over a non-planar geometry. On the left, we observe their slip distributions. On the right, we show the resulting vertical displacement fields

We computed the average coastal amplitude of all 99 stochastic scenarios for each seismic gap (Fig. 14). The ratio of the mean stochastic amplitude to the uniform amplitude was then obtained. For TGap, a mean ratio of 1.25 with a standard deviation of 0.17 was determined. However, this ratio can reach values of up to 2.24. Secondly, GGap shows a mean ratio equal to 1.31 with a standard deviation of 0.22. The maximum underestimation factor for this gap is 2.17. Finally, JGap shows a mean underestimation factor of 1.38 with a standard deviation and maximum value of 0.26 and 2.58, respectively. Thus, on average, one can expect that when an uniform slip distribution is assumed rather than a stochastic slip distribution, there will an underestimation factor of approximately 1.3 in the final coastal amplitudes, e.g., when a coastal amplitude of 2 m is computed

from an uniform slip distribution, a more realistic value should be 2.6 m. However, a larger underestimation will be obtained when we only consider the maximum stochastic scenarios is 2, thus, the coastal amplitudes generated by these extreme cases are approximately 4 m. These differences are intrinsically due to the internal structure of the sources that are being assumed. As discussed by Geist and Dmowska (1999), the local tsunami wavefield is dependent on variations of slip. Because the vertical displacement is translated as the initial condition of tsunami propagation and because this displacement field is directly dependent on the slip gradient, variation of the slip in the dip direction must be accounted for. Furthermore, local tsunami coastal amplitudes generated by $7 < M_w < 8.5$ earthquakes are highly variable (Geist, 2002). Such variations can

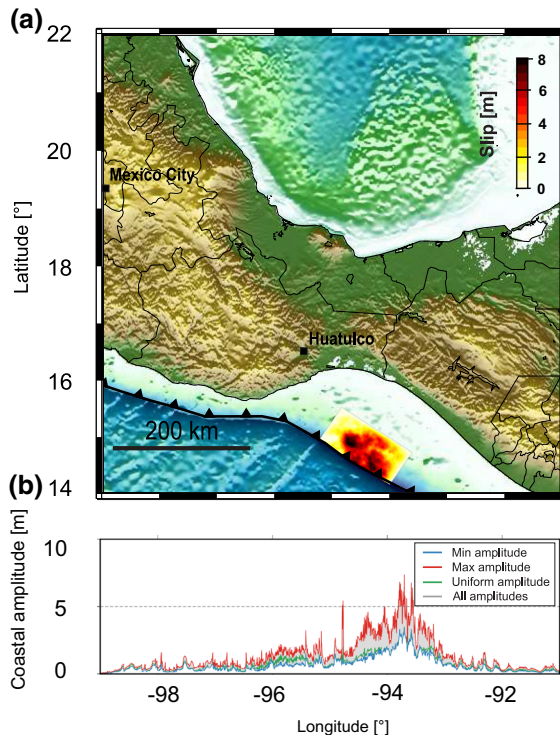


Figure 9

Complete set of coastal amplitudes for 99 numerical simulations of tsunami propagation in TGap. **a** Region of Mexico where the numerical simulation were computed. **b** Visualization of the minimum (lower black line), maximum (upper black line), and the more probable (red dots) amplitudes computed in this study

be ascribed to, among others, heterogeneities in the slip distribution.

As previously pointed out, our study focuses on numerical simulations of three hypothetical megathrust earthquakes, and a number of other factors, which we did not take into account, could affect the coastal inundation computations in the near field, these factors as mentioned in Ruiz et al. (2015) include (1) horizontal displacements of the seabed, (2) high-resolution bathymetry near the shore, (3) the dynamic displacement of the seafloor caused by the space-time rupture process. We additionally think that a more detailed bathymetry in our study zones would improve our numerical simulations and, thus, our coastal amplitude results would be more accurate. However, Borrero et al. (1997) and Trejo-Gómez et al. (2015) reported run-ups ranging from 1 to 5 m for the 1995 Jalisco-Colima Mw 8.0 earthquake. Ramírez-Herrera et al. (2015) reported historical run-

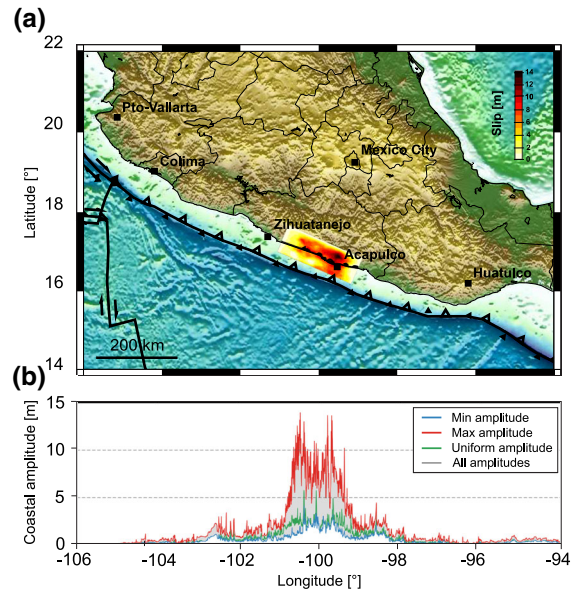


Figure 10

Complete set of coastal amplitudes for 99 numerical simulations of tsunami propagation in GGAP. **a** Region of Mexico where the numerical simulation were computed. **b** Visualization of the minimum (blue line), maximum (red line), the remaining stochastic (gray area), and the uniform (green line) amplitudes computed in this study

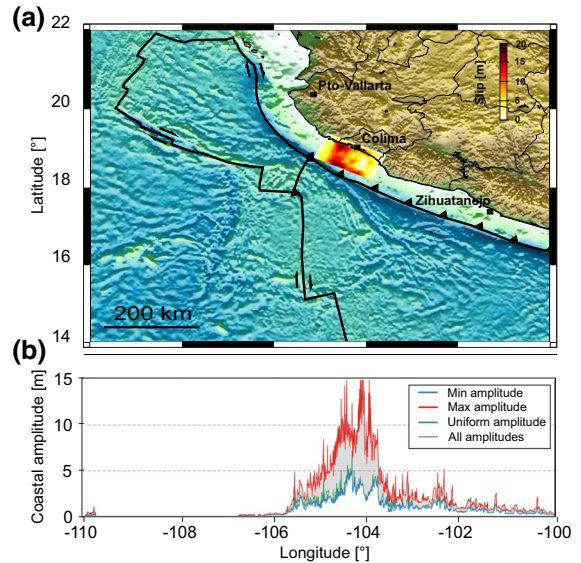


Figure 11

Complete set of coastal amplitudes for 100 numerical simulations of tsunami propagation in JGap. **a** Region of Mexico where the numerical simulation were computed. **b** Visualization of the minimum (blue line), maximum (red line), the remaining stochastic (gray area), and the uniform (green line) amplitudes computed in this study

up measurements ranging from 0.2 to 11 m in Zihuatanejo, Acapulco, and Ixtapa. We thus consider our results to be congruent with these run-up estimates, i.e., our hypothetical $M_w 8.2$ JGap and GGap events produced mean coastal amplitudes from 6 to 8 m and from 4 to 6 m, respectively.

We also compare our numerical results against an empirical law proposed by Plafker (1997). The Plafker's Law states that, if there are not abrupt changes in the topography along the coastline, the range of the maximum coastal amplitudes is in the order of the maximum co-seismic slip and it cannot be more than twice the co-seismic peak-slip at the source. Rosenau et al. (2010) showed that the coastal

►
Figure 13
Coastal amplitude distributions along the coastline of **a** the Tehuantepec seismic gap, **b** the Guerrero seismic gap, and **c** the Colima–Jalisco seismic gap. A log normal distribution was fitted in each case following a Chi-squared test, where c.v. is the empirical coefficient of variation and c.v._{LN} is the coefficient of variation of the log normal distribution

amplitude scales linearly with the slip at the source. Our numerical results obey these rules of thumb, as shown in Fig. 15. We observe that the maximum coastal amplitudes scale linearly with the maximum slips by a factor between 0.50 and 0.72 in the

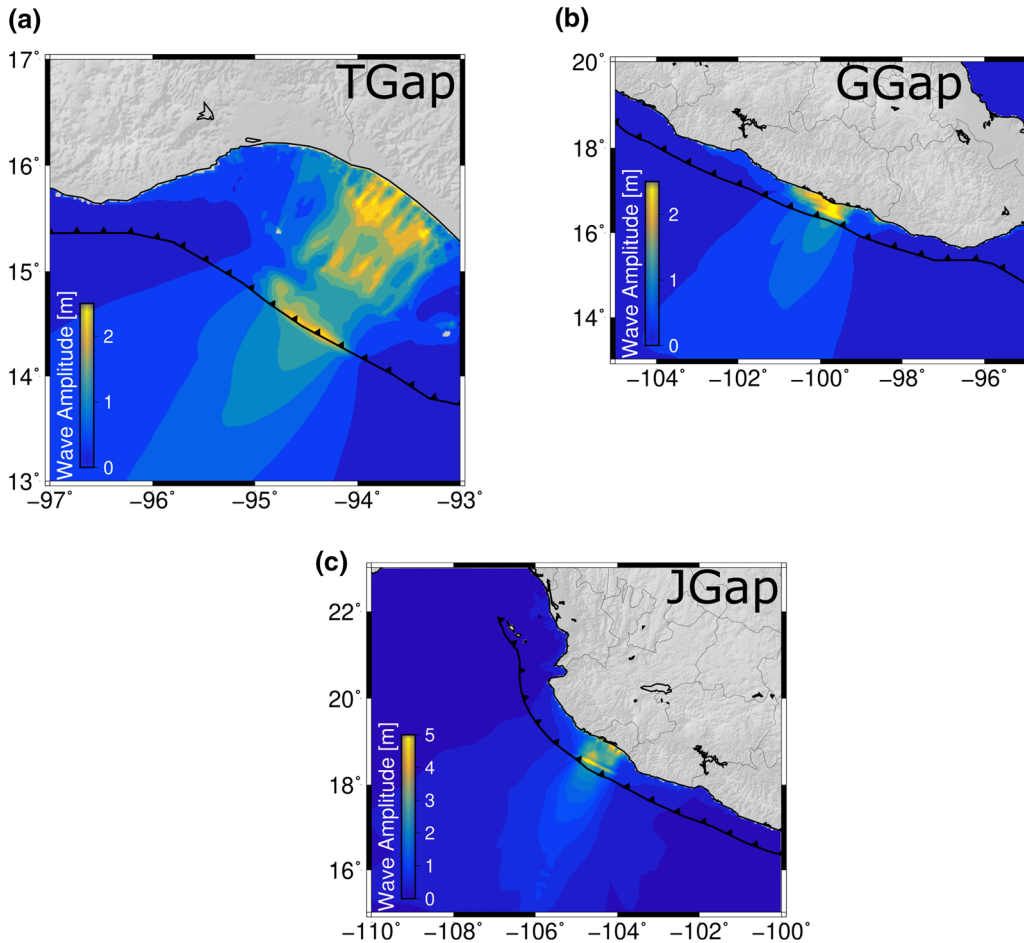
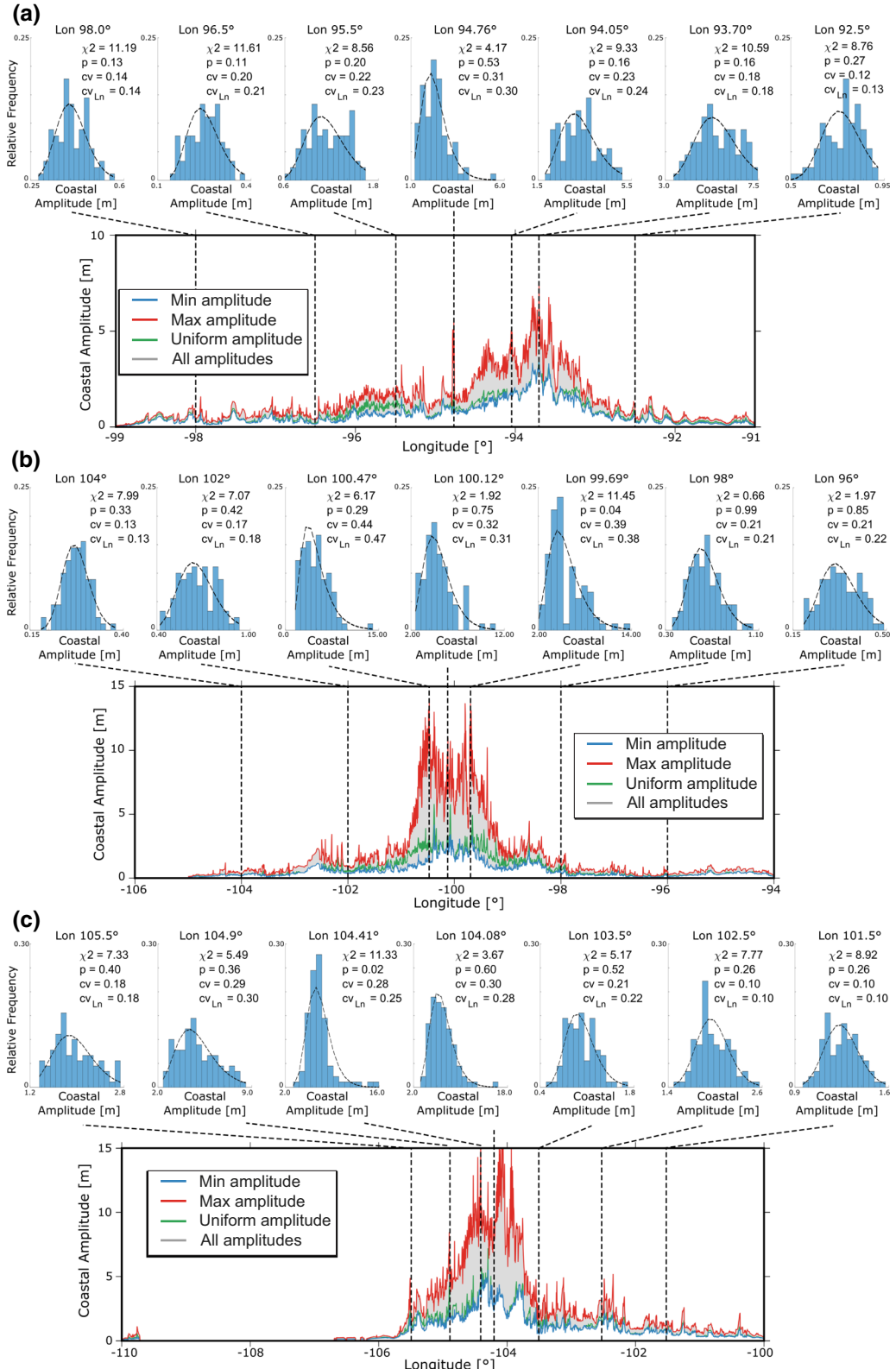


Figure 12

Tsunami wavefield for the stochastic scenario 45 after 6 h of computation for the tsunami propagation. **a** Oceanic waves amplitudes for the Tehuantepec seismic gap. **b** Oceanic waves amplitudes for the Guerrero seismic gap. **c** Oceanic waves amplitudes for the Colima–Jalisco seismic gap

Numerical Simulation of Tsunami Coastal Amplitudes in the Pacific Coast



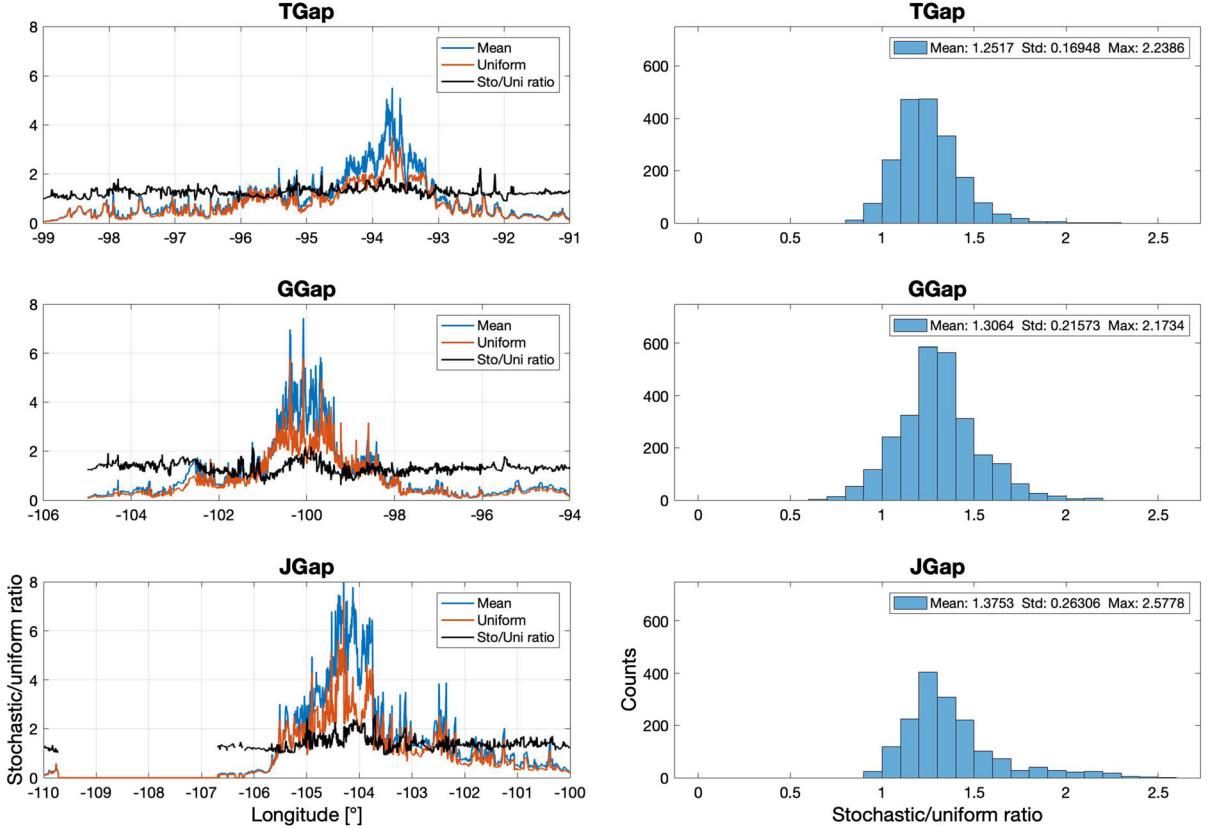


Figure 14

Coastal amplitude distributions along the coastline of the three proposed seismic gaps. The average values are shown in blue, the uniform distributions are depicted in orange, and the ratio of the stochastic average amplitude to the uniform amplitude is shown in black. The three right sub-panels show the distributions of this ratio

simulations for the three hypothetical seismic scenarios. Our results show that the maximum amplitudes are in the order of the maximum co-seismic slip, therefore, the simulated peak-amplitudes versus peak-slip obey Palfker's Law, thus, our numerical simulations agree with the tsunami and earthquake physics and empirical observations. Only for comparison purposes, the 1995 Mexico and 2015 Illapel megathrust earthquakes generated slip values of 5 m (Hutten et al. 2001) and 8 m (Melgar et al. 2016), and the maximum amplitudes of 10 m (Borrero et al. 1997), and 11.4 m (Fuentes et al. 2016), respectively. We can also make comparisons between the results of GGap and JGap, mainly because the earthquakes in both gaps are of the same magnitude. The former showed smaller values in slip and coastal amplitudes than the latter, thus, an earthquake in the Colima–

Jalisco gap would generate a larger tsunami than an earthquake of the same magnitude in the Guerrero gap.

Some historical tsunami records are still under debate. For instance, while some authors suggest that the 10 m tsunami generated by the 1932 M 6.9 earthquake in Jalisco is the result of a submarine slump (Corona and Ramírez-Herrera, 2015), Okal and Borrero (2011) suggest that this seismic event was a tsunami earthquake, thus producing such high amplitude. Additionally, Ramírez-Herrera et al. (2015) reported 11 m values in Zihuatanejo generated by the 1925 M_s 7.0 seismic event (Table 1); however, Singh et al. (1998) suggested that due to the large distance between Zihuatanejo and the seismic epicenter (600 km), this high amplitude was generated by a submarine slump near Zihuatanejo, alternatively,

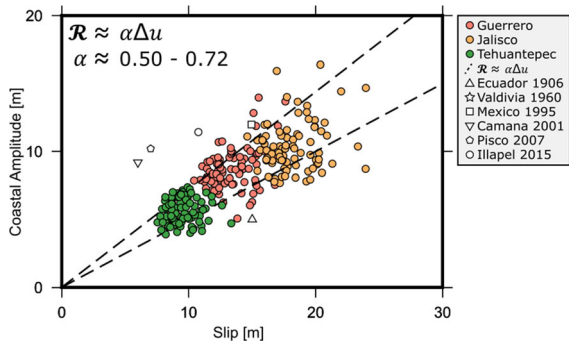


Figure 15

Plafker's rule of thumb. Simulated near-field peak coastal amplitudes compared against the maximum co-seismic slip at the source (green, red, and orange dots for TGap, GGap, and JGap, respectively). The straight lines represent the bounds of the data linear fit. Other symbols specified in the legend are used for comparison only

the authors suggested a meteorological source as well. These discrepancies may suggest that whether large tsunamis can hit the Pacific Coast of Mexico or not cannot be answered yet; however, a recent study by Ramírez-Herrera et al. (2020) showed that larger earthquake and tsunamis than previously thought have whipped the coasts of Guerrero and Oaxaca in Mexico. The oldest one struck the Pacific Coast of Mexico in 1537, and then, in 1787 a second large documented earthquake hit, suggesting a recurrence interval of 250 years. This study demonstrated that the common belief that large tsunamis do not occur along the Pacific Coast of Mexico cannot be preserved. Our study reinforces this hypothesis, showing plausible large coastal amplitudes in three different seismic gaps in Mexico.

4. Conclusions

In this study, we simulated three hypothetical seismic gaps along the Pacific Coast of Mexico. Their magnitudes and rupture areas are fixed in our numerical models, where the formers were chosen according to historical seismicity and rupture area dimensions. We then generated a set of stochastic slip distributions built-up under the frame of physics-based earthquake source models. Under the passive tsunami generation framework, we modeled the tsunami and its variation along the coast. While we

acknowledge that our simulations can be improved by using finer and better detailed bathymetry and by considering other factors previously described, our results are not distant from what historical records show (Borrero et al., 1997; Ramírez-Herrera et al., 2015; Trejo-Gómez et al., 2015; Ramírez-Herrera et al., 2020).

One of our goals was to determine the underestimation factor generated by an uniform slip distribution assumption over stochastic scenarios. It was shown that this factor is on average 1.3 for the three seismic gaps presented in this study. As pointed out by Geist and Dmowska (1999) and Geist (2002), local tsunami coastal amplitudes are strongly affected by the heterogeneity of seismic sources. Our results support such studies.

Extreme coastal amplitudes are described in great detail in this study. Even though such values are rare, one resolution out of 99 scenarios, previous studies have shown the plausibility of large tsunamis hitting the coasts of Mexico (Ramírez-Herrera et al., 2020). Our analysis suggests that these coastal amplitudes are physically possible. It is thus the decision makers' and general population's responsibility, to be prepared in case of a tsunami warning. Special care should be taken for the coastal towns in Mexico that might be affected by such large tsunamis, e.g., Huatulco, Puerto Angel, Acapulco, Zihuatanejo, Manzanillo, Puerto Vallarta, just to mention some. We cannot predict earthquakes nor tsunamis; however, we can mitigate the risk by educating the population on the required actions that must be taken in presence of these events. According to the National Tsunami Hazard Mitigation Program in the United States of America, pertinent protective measures in case of a tsunami include, for instance, planning and practicing for response to tsunamis; warning the public, establishing, marking, and publicizing evacuation routes; and educating the public, residents and visitors, about this phenomenon before it strikes. It is important to note that the results presented in this study are by no means tsunami hazard (nor risk) assessments, thus, our work cannot be used for tsunami response and emergency evacuation planning, and for any other tsunami mitigation measures, including land-use regulations.

Acknowledgements

Some figures were drawn using Generic Mapping Tools (GMT) version 4.0 (Wessel and Smith 1998). This work was funded by Secretaría de Educación Pública (SEP) under the program Métodos de Investigación. We also thank Dr. Yoshiki Yamazaki who facilitated the use of his code, NEOWAVE.

Funding

This work was funded by Secretaría de Educación Pública, México (SEP). This Mexican government agency afforded the flights, lodging, and food for Luis Vazquez in Santiago, Chile. This award is assigned to undergrad students at Universidad Nacional Autónoma de México.

Availability of data and material

Not applicable.

Code application

This work was done using Matlab.

Declarations

Conflict of interest Not applicable.

Publisher's Note Springer Nature remains neutral with regard to jurisdictional claims in published maps and institutional affiliations.

REFERENCES

- Abe, K., Hakuno, M., Takeuchi, M., & Katada, T. (1986). Survey report on the tsunami of the Michoacan, Mexico earthquake of September 19, 1985. *Bulletin of Earthquake Research Institute*, 61, 475–481.
- Aki, K. (1967). Scaling law of seismic spectrum. *Journal of Geophysical Research*, 72(4), 1217–1231.
- Andrews, D. J. (1980). A stochastic fault model: 1. Static case. *Journal of Geophysical Research: Solid Earth*, 85(B7), 3867–3877.
- Becker, J. J., Sandwell, D. T., Smith, W. H. F., Braud, J., Binder, B., Depner, J., et al. (2009). Global bathymetry and elevation data at 30 arc seconds resolution. *Marine Geodesy*, 32(4), 355–371.
- Blaser, L., Krüger, F., Ohrnberger, M., & Scherbaum, F. (2010). Scaling relations of earthquake source parameter estimates with special focus on subduction environment. *Bulletin of the Seismological Society of America*, 100(6), 2914–2926.
- Borero, J., Ortiz, M., Titov, V., & Synolakis, C. (1997). Field survey of Mexican tsunami produces new data, unusual photos. *Eos, Transactions American Geophysical Union*, 78(8), 85–88.
- Corona, N., & Ramírez-Herrera, M. T. (2012). Mapping and historical reconstruction of the great Mexican 22 June 1932 tsunami. *Natural Hazards and Earth System Sciences*, 12(5), 1337–1352.
- Corona, N., & Ramírez-Herrera, M. T. (2015). Did an underwater landslide trigger the June 22, 1932 tsunami off the Pacific coast of Mexico? *Pure and Applied Geophysics*, 172(12), 3573–3587.
- Cruz-Atienza, V. M., Ito, Y., Kostoglodov, V., Hjörleifsdóttir, V., Iglesias, A., Tago, J., et al. (2018). A seismogeodetic amphibious network in the Guerrero seismic gap, Mexico. *Seismological Research Letters*, 89(4), 1435–1449.
- Farreras, S. (1997). Tsunamis en Mexico. In *Contribuciones a la Oceanografia Fisica en Mexico*, Monografia No. 3 (pp. 73–96). Union Geofisica Mexicana.
- Franco, A., Lasserre, C., Lyon-Caen, H., Kostoglodov, V., Molina, E., Guzman-Speziale, M., et al. (2012). Fault kinematics in northern Central America and coupling along the subduction interface of the Cocos Plate, from GPS data in Chiapas (Mexico), Guatemala and El Salvador. *Geophysical Journal International*, 189(3), 1223–1236.
- Fuentes, M., Riquelme, S., Hayes, G., Medina, M., Melgar, D., Vargas, G., et al. (2016). A study of the 2015 M w 8.3 Illapel earthquake and tsunami: Numerical and analytical approaches. *Pure and Applied Geophysics*, 173, 1847–1858.
- Fujii, Y., Satake, K., Sakai, S. I., Shinohara, M., & Kanazawa, T. (2011). Tsunami source of the 2011 off the Pacific coast of Tohoku earthquake. *Earth, Planets and Space*, 63(7), 815–820.
- Gallovic F., & Brokesová, J. (2004). On strong ground motion synthesis with k^{-2} slip distributions. *Journal of Seismology*, 8(2), 211–224.
- García, V., & Suárez, G. (1996). *Los Sismos en la Historia de México*. México: Universidad Nacional Autónoma de México Press.
- Geist, E. L. (2002). Complex earthquake rupture and local tsunamis. *Journal of Geophysical Research*, 107(B5), 2086.
- Geist, E. L., & Dmowska, R. (1999). Local tsunamis and distributed slip at the source. *Seismogenic and tsunamigenic processes in shallow subduction zones* (pp. 485–512). Basel: Birkhauser.
- Gripp, A. E., & Gordon, R. G. (2002). Young tracks of hotspots and current plate velocities. *Geophysical Journal International*, 150(2), 321–361.
- Gusman, A. R., Mulia, I. E., & Satake, K. (2018). Optimum sea surface displacement and fault slip distribution of the 2017 Tehuantepec earthquake (Mw 8.2) in Mexico estimated from tsunami waveforms. *Geophysical Research Letters*, 45(2), 646–653.
- Hayes, G. (2018). Slab2—A comprehensive subduction zone geometry model. *Science*, 362(6410), 10–58.

- Herrero, A., & Bernard, P. (1994). A kinematic self-similar rupture process for earthquakes. *Bulletin of the Seismological Society of America*, 84(4), 1216–1228.
- IDE, S., Baltay, A., & Beroza, G. C. (2011). Two faces of the great Tohoku earthquake: Shallow dynamic overshoot and energetic deep rupture. *Science*, 332(6036), 1426–1429.
- Kostoglodov, V., & Pacheco, J. F. (1999). One hundred years of seismicity in Mexico. Inst. de Geofisica., Universidad Nacional Autonoma de Mexico (UNAM), Mexico City.
- Lay, T., Ammon, C. J., Kanamori, H., Xue, L., & Kim, M. J. (2011). Possible large near-trench slip during the 2011 M_w 9.0 off the Pacific coast of Tohoku earthquake. *Earth Planets and Space*, 63, 32.
- Lay, T., Ye, L., Kanamori, H., Yamazaki, Y., Cheung, K. F., & Ammon, C. J. (2013). The February 6, 2013 Mw 8.0 Santa Cruz Islands earthquake and tsunami. *Tectonophysics*, 608, 1109–1121.
- Mai, P. M., & Beroza, G. C. (2002). A spatial random field model to characterize complexity in earthquake slip. *Journal of Geophysical Research*, 107(B11), 2308.
- Melgar, D., Allen, R. M., Riquelme, S., Geng, J., Bravo, F., Baez, J. C., et al. (2016). Local tsunami warnings: Perspectives from recent large events. *Geophysical Research Letters*, 43(3), 1109–1117.
- Melgar, D., Ruiz-Angulo, A., Garcia, E. S., Manea, M., Manea, V. C., Xu, X., et al. (2018). Deep embrittlement and complete rupture of the lithosphere during the M w 8.2 Tehuantepec earthquake. *Nature Geoscience*, 11(12), 955–960.
- Melgar, D., Williamson, A. L., & Salazar-Monroy, E. F. (2019). Differences between heterogenous and homogenous slip in regional tsunami hazards modelling. *Geophysical Journal International*, 219(1), 553–562.
- Melgar, D., Ruiz-Angulo, A., Pérez-Campos, X., Crowell, B. W., Xu, X., Cabral-Cano, E., et al. (2021). Energetic Rupture and Tsunamigenesis during the 2020 M w 7.4 La Crucecita, Mexico earthquake. *Seismological Society of America*, 92(1), 140–150.
- Moreno, M., Rosenau, M., & Oncken, O. (2010). 2010 Maule earthquake slip correlates with pre-seismic locking of Andean subduction zone. *Nature*, 467(7312), 198–202.
- Núñez-Cornú, F. J., Sandoval, J. M., Alarcón, E., Gómez, A., Suárez-Plascencia, C., Núñez, D., & Zúñiga-Medina, L. M. (2018). The Jalisco seismic accelerometric telemetric network (RESAJ). *Seismological Research Letters*, 89(2A), 363–372.
- Okada, Y. (1992). Internal deformation due to shear and tensile faults in a half-space. *Bulletin of the Seismological Society of America*, 82(2), 1018–1040.
- Okal, E. A., & Borrero, J. C. (2011). The ‘tsunami earthquake’ of 1932 June 22 in Manzanillo, Mexico: seismological study and tsunami simulations. *Geophysical Journal International*, 187(3), 1443–1459.
- Ortiz, M., Singh, S. K., Pacheco, J., & Kostoglodov, V. (1998). Rupture length of the October 9, 1995 Colima–Jalisco Earthquake (Mw 8) estimated from tsunami data. *Geophysical Research Letters*, 25(15), 2857–2860.
- Ortiz, M., Kostoglodov, V., Singh, S. K., & Pacheco, J. (2000). New constraints on the uplift of October 9, 1995 Jalisco–Colima earthquake (M_w 8.0) based on the analysis of tsunami records at Manzanillo and Navidad, Mexico. *Geofísica Internacional*, 39(4), 349–357.
- Pardo, M., & Suárez, G. (1995). Shape of the subducted Rivera and Cocos plates in southern Mexico: Seismic and tectonic implications. *Journal of Geophysical Research: Solid Earth*, 100(B7), 12357–12373.
- Plafker, G. (1997). Catastrophic tsunami generated by submarine slides and backarc thrusting during the 1992 earthquake on eastern Flores I., Indonesia. *Geological Society of America Cordillera Section*, 29(5), 57.
- Poisson, B., Oliveros, C., & Pedreros, R. (2011). Is there a best source model of the Sumatra 2004 earthquake for simulating the consecutive tsunami? *Geophysical Journal International*, 185(3), 1365–1378.
- Ramírez-Herrera, M. T., Corona, N., & Suárez, G. A. (2015). *Review of Great Magnitude Earthquakes and associated tsunamis along the Guerrero, Mexico Pacific Coast: A multiproxy approach* (pp. 165–176). *Geophysical Research Letters*.
- Ramírez-Herrera, M. T., Corona, N., Ruiz-Angulo, A., Melgar, D., & Zavala-Hidalgo, J. (2018). The 8 September 2017 tsunami triggered by the Mw 8.2 intraplate earthquake, Chiapas, Mexico. *Pure and Applied Geophysics*, 175(1), 25–34.
- Ramírez-Herrera, M. T., Corona, N., Cerny, J., Castillo-Aja, R., Melgar, D., Lagos, M., et al. (2020). Sand deposits reveal great earthquakes and tsunamis at Mexican Pacific Coast. *Scientific Reports*, 10(1), 1–10.
- Riquelme, S., Schwarze, H., Fuentes, M., & Campos, J. (2020). Near-field effects of earthquake rupture velocity into tsunami runup heights. *Journal of Geophysical Research: Solid Earth*, 125(6), e2019JB018946.
- Rosenau, M., Nerlich, R., Brune, S., & Oncken, O. (2010). Experimental insights into the scaling and variability of local tsunamis triggered by giant subduction megathrust earthquakes. *Journal of Geophysical Research: Solid Earth*, 115(B9).
- Ruiz, J., Baumont, D., Bernard, P., & Berge-Thierry, C. (2007). New approach in the kinematic k^2 source model for generating physical slip velocity functions. *Geophysical Journal International*, 171(2), 739–754.
- Ruiz, J. A., Fuentes, M., Riquelme, S., Campos, J., & Cisternas, A. (2015). Numerical simulation of tsunami runup in northern Chile based on non-uniform k^2 slip distributions. *Natural Hazards*, 79(2), 1177–1198.
- Sánchez, A. J., & Farreras, S. F. (1993). *Catalog of Tsunamis on the Western Coast of Mexico* (p. 79). Boulder: National Geophysical Data Center.
- Santos-Reyes, J. (2020). *The Risk of Tsunamis in Mexico*. In: *Natural Hazards-Impacts, Adjustments and Resilience*. IntechOpen.
- Simons, M., Minson, S. E., Sladen, A., Ortega, F., Jiang, J., Jiang, J., et al. (2011). The 2011 magnitude 9.0 Tohoku-Oki earthquake: Mosaicking the megathrust from seconds to centuries. *Science*, 332(6036), 1421–1425.
- Singh, S. K., Astiz, L., & Havskov, J. (1981). Seismic gaps and recurrence periods of large earthquakes along the Mexican subduction zone: A reexamination. *Bulletin of the Seismological Society of America*, 71(3), 827–843.
- Singh, S. K., Pacheco, J. F., & Shapiro, N. (1998). The earthquake of 16 November, 1925 (M_s = 7.0) and the reported tsunami in Zihuatanejo, Mexico. *Geofísica Internacional*, 37(1), 0.
- Smith, W. H. T., & Sandwell, T. D. (1997). Global sea floor topography from satellite altimetry and ship depth soundings. *Science*, 277, 1956.
- Suárez, G., & Albini, P. (2009). Evidence for great tsunamigenic earthquakes (M 8.6) along the Mexican subduction zone. *Bulletin of the Seismological Society of America*, 99(2A), 892–896.

- Synolakis, C. E., Bernard, E. N., Titov, V. V., Kânoğlu, U. T. K. U., & Gonzalez, F. I. (2008). Validation and verification of tsunami numerical models. *Tsunami science four years after the 2004 Indian Ocean tsunami* (pp. 2197–2228). Basel: Birkhäuser.
- Trejo-Gómez, E., Ortíz, M., & Núñez-Cornú, F. J. (2015). Source Model of the October 9, 1995 Jalisco–Colima Tsunami as constrained by field survey reports, and on the numerical simulation of the tsunami. *Geofísica Internacional*, 54(2), 149–159.
- Williamson, A., Melgar, D., & Rim, D. (2019). The effect of earthquake kinematics on tsunami propagation. *Journal of Geophysical Research: Solid Earth*, 124(11), 11639–11650.
- Yagi, Y., & Fukahata, Y. (2011). Rupture process of the 2011 Tohoku–Oki earthquake and absolute elastic strain release. *Geophysical Research Letters*, 38(19).
- Yamazaki, Y., & Cheung, K. F. (2011). Shelf resonance and impact of near-field tsunami generated by the 2010 Chile earthquake. *Geophysical Research Letters*, 38(12).
- Yamazaki, Y., Cheung, K. F., & Kowalik, Z. (2011a). Depth-integrated, non-hydrostatic model with grid nesting for tsunami generation, propagation, and run-up. *International Journal for Numerical Methods in Fluids*, 67, 2081–2107.
- Yamazaki, Y., Lay, T., Cheung, K. F., Yue, H., & Kanamori, H. (2011b). Modeling near-field tsunami observations to improve finite-fault slip models for the 11 March 2011 Tohoku earthquake. *Geophysical Research Letters*, 38(7).
- Yamazaki, Y., Kowalik, Z., & Cheung, K. F. (2009). Depth-integrated, non-hydrostatic model for wave breaking and run-up. *International Journal for Numerical Methods in Fluids*, 61(5), 473–497.
- Yoshida, K., Miyakoshi, K., & Irikura, K. (2011). Source process of the 2011 off the Pacific coast of Tohoku earthquake inferred from waveform inversion with long-period strong-motion records. *Earth Planets and Space*, 63(7), 577–582.

(Received August 24, 2020, revised May 19, 2021, accepted June 11, 2021)